

Analysis of Mechanical Characteristics and Instability Law of Fault under the Influence of Mining

Yuanhui Li¹, Rui Zhou^{1,2*}

¹Key Laboratory of Ministry of Education on Safe Mining of Deep Metal Mines, Northeastern University, Shenyang 110819, P.R. China.

²China Coal Technology Engineering Group, Shenyang Research Institute, Shenyang 110016, P.R. China.

* Email of corresponding author: 3416197979@qq.com

ABSTRACT

An inverse mechanics model has been built under work face mining conditions, according to the law of working surface pressure distribution, to explore the mechanical characteristics and stability of the reverse fault under the influence of mining. As a result, a theoretical calculation equation of the normal and shear stresses in the fault zone has been deduced to obtain the stress variation rule between the working surface and the fault layer, under distance conditions of 10, 30, 50, and 70m. With distance conditions of 10 and 30m, the working surface mining stress had a noticeable effect on the reverse fault, resulting in a changing trend of firstly increasing, then decreasing, and increasing again in the normal and shear stresses of the fault zone as a whole. With distance conditions of 50 and 70m, the working face mining stress had little effect on the reverse fault; furthermore, the normal and shear stresses exhibited a changing trend of gradually increasing. At a later stage, a simulation of the above distance plans was conducted using the FLAC3D numerical simulation software. The results demonstrated that the influence range of the mining stress on the working face under the spacing distances of 10 and 30m included the fault zone, while under the distance conditions of 50 and 70m, the fault zone was excluded. On this basis, the fault zone stability was analyzed under four types of spacing conditions using the Mohr-Coulomb theory rule and fault activation determination. It is concluded that the fault zone stability was high, with increasing distances between the working face and fault zone. The least sufficient stability was located near the working face, where the fault zone stability was so weak that it is likely to result in impact fracture.

Keywords: Reverse fault; Normal stress; Shear stress; Fault instability; Rock burst;

Análisis de las características mecánicas y las condiciones de inestabilidad de fallas en áreas de explotación minera

RESUMEN

Se construyó un modelo mecánico inverso bajo las condiciones de un frente de trabajo minero, de acuerdo con las condiciones de distribución de presión en la superficie de operación, para explorar las características mecánicas y la estabilidad de la falla inversa en estas áreas de explotación minera. Como resultado, se dedujo una ecuación teórica para calcular el esfuerzo normal y el esfuerzo cortante en la zona de falla y con el fin de obtener el régimen de variación de esfuerzos entre la superficie de trabajo y la capa de la falla a distancias de 10, 30, 50 y 70 metros. A 10 y 30 metros de distancia, el esfuerzo en la zona de trabajo tiene un efecto notorio en la falla inversa, lo que significa un cambio en la tendencia de los esfuerzos normal y cortante, que primero se incrementan, decrecen y nuevamente aumentan en toda la zona de la falla. A 50 y 70 metros, el esfuerzo en el frente de trabajo tiene poco efecto en la falla inversa; además, los esfuerzos normal y cortante mostraron una tendencia cambiante de crecimiento gradual. Por último, se realizó una simulación en cada una de las distancias con el software de simulación numérica FLAC3D. Los resultados demuestran que el rango de influencia del esfuerzo en el frente de trabajo a distancia de 10 y 30 metros incluyen la zona de falla, mientras que a 50 y 70 metros la zona de falla está excluida. De acuerdo con estos resultados, se analizó la estabilidad de la zona de falla en cuatro condiciones de espacio con la teoría de Mohr-Coulomb y la determinación de activación de falla. Se concluye que la estabilidad en la zona de falla es mayor con el incremento de las distancias entre el frente de trabajo y la zona de falla. El menor punto de estabilidad suficiente se ubicó cerca del frente de trabajo, donde la estabilidad de la zona de falla es tan baja que podría derivar en una fractura de impacto.

Palabras clave: Falla inversa; Esfuerzo Normal; Esfuerzo Cortante; Inestabilidad de Falla; Explosión rocosa.

Record

Manuscript received: 14/11/2017

Accepted for publication: 11/06/2018

How to cite item

Li, Y., & Zhou, R. (2018). Analysis of Mechanical Characteristics and Instability Law of Fault under the Influence of Mining. *Earth Sciences Research Journal*, 22(2), 139-144.

DOI: <http://dx.doi.org/10.15446/esrj.v22n2.72249>

1 Introduction

Coal reserves of 1.48 trillion tons have been identified in China, ranking third in the world. However, coal seams are buried deeply, with many folds, faults, and other geological structures, particularly in the tectonic region of fault. The damaged continuity of coal and rock seams poses a challenge to coal mining (Tan et al., 2011; Xiao et al., 2016; Sufiyan et al., 2018). Moreover, fault instability generated by the coal mining influence in areas affected by the fault structure may result in disasters such as rock bursts (Li et al., 2014; Rahim et al., 2018; Mahmood et al., 2018), water inrush through the fault (LaMoreaux, Wu, & Zhou, 2014; Khanchoul et al., 2018), and coal and gas outbursts (Diaz-Aguado, & González-Nicieza, 2007). The changing law of mining mechanics under the influence of fault has always been the focus of rock burst prevention, particularly in the prevention and control of rock burst. Gibowicz (1984) and McGarr (1984) determined that an ore quake is similar to a natural earthquake source mechanism, and shear slip in the fault zone mainly causes large-energy mine earthquakes. The majority of theories regarding the seismic source mechanism can be used for mine earthquakes. Joughin and Jager (1984), Potgieter and Roering (1984) discovered that large-energy mine earthquakes are closely related to shear slip in their study of a mine earthquake that occurred in a particular South African gold mine. Chinese scholars Jiang and Liu (2010) proposed a correlation between different fault types and rock burst occurrences. These are more likely to occur in the pressure bump when the working surface is overtaken by the reverse fault, according to data prepared by Jiang et al. (2014).

It is concluded that a rock burst induced by the reverse fault is more likely to accumulate a significant amount of elastic energy with strong destruction, upon conducting a statistical analysis of a rock burst disaster induced by the reverse fault. Through micro-seismic, electromagnetic radiation and other equipment, it is possible to monitor the fact that a mechanical indication in some form occurs before the rock burst induced by the reverse fault, and such that evidence serves as identification of fault instability (Veeraragavan et al., 2018; Nwankwoala & Ememu, 2018). Although various scholars have studied the phenomenon, the majority of studies have focused mainly on field monitoring data analysis. Less analysis has carried out on the theoretical causes of this mechanical indication, and the changing law of the standard and shear stresses causing the evidence in the fault zone. Therefore, according to the actual geological characteristics of the mining face under the influence of a mining area's reverse fault, the distribution law of the supporting pressure in the coal seam direction is analyzed in this paper (Sudhakaran et al., 2018; Guan Leong et al., 2018). Moreover, a mechanics model of the stope has been established under the reverse fault to explore the pressure changing laws and instability of the reverse fault under the mining influence, providing a reference for the prevention and control of the pressure bump induced by the reverse mistake (Wali et al., 2018).

2. Materials and methods

2.1. Mechanics model of the working surface trending to the reverse fault

The tendency of the mining working face of the coal seam in a mining area to be affected by the F16 reverse fault was evaluated. The thickness of the coal seam is 5m; the upper roof of the coal seam is a conglomerate of 190m in diameter, and the fault angle is 60°. After the mining face, the overlying strata are collapsed. Assuming that the stratigraphic coal and rock mass are an isotropic elastic body, the top plate plane would be taken above the working surface. The pressure distribution of the overlying strata trending along the working surface is shown in Fig. 1 (Qian, 2003; Thiruchelvam et al., 2018; Tair & Dell, 2018).

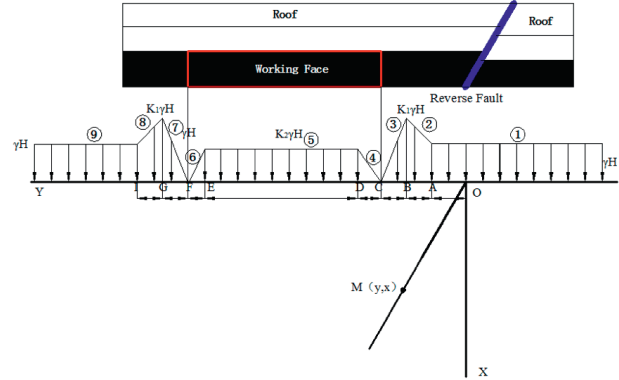


Figure 1. Pressure distribution along working face

The pressure of the $-\infty$ to A and I to $+\infty$ zones indicate the stress of the original rock γH . AI is the stress affecting the working face zone, where AB, BC, FG, and GI are the stress increasing zones (simplified as a linear increase). Furthermore, CD, DE, and EF are the stress reduction zones (simplified as a linear decrease). The intersection of the fault and the roof plane is the origin O, while the angle with the Y-axis is the dip angle θ of the fault (Asghar et al., 2018). The working surface is at point c, the working face stress concentration coefficient is K_1 , and the working face stress reduction coefficient is K_2 .

According to elastic mechanics theory, the stress of a point M (y, x) on the fault can be obtained as follows:

$$\sigma_x = \frac{-2}{\pi} \left(\int_a^c \frac{\gamma \cdot H \cdot x^2}{[x^2 + (y-\xi)^2]^2} d\xi + \int_c^e \frac{(\gamma \cdot H - K_1 \cdot \gamma \cdot H \cdot \xi - \frac{B \cdot \gamma \cdot H - K_1 \cdot h \cdot \gamma \cdot A}{A-B} \cdot x^2)}{[x^2 + (y-\xi)^2]^2} d\xi + \int_e^g \frac{(\frac{K_1 \cdot \gamma \cdot H \cdot \xi - K_1 \cdot j \cdot \gamma \cdot C}{B-C} \cdot x^2)}{[x^2 + (y-\xi)^2]^2} d\xi + \int_g^i \frac{(\frac{-K_2 \cdot \gamma \cdot H \cdot \xi + \frac{H \cdot \gamma \cdot C \cdot K_2}{C-D} \cdot x^2)}{[x^2 + (y-\xi)^2]^2} d\xi + \int_i^o \frac{(\frac{K_2 \cdot \gamma \cdot H \cdot x^2 - K_2 \cdot F \cdot \gamma \cdot H}{E-F} \cdot x^2)}{[x^2 + (y-\xi)^2]^2} d\xi + \int_o^{\infty} \frac{(\frac{-K_1 \cdot \gamma \cdot H \cdot \xi + \frac{K_1 \cdot F \cdot \gamma \cdot H}{F-G} \cdot x^2)}{[x^2 + (y-\xi)^2]^2} d\xi + \int_o^{\infty} \frac{(\frac{(\gamma \cdot H - K_1 \cdot \gamma \cdot H \cdot \xi + \frac{G \cdot \gamma \cdot H - K_1 \cdot l \cdot \gamma \cdot H}{G-I} \cdot x^2)}{[x^2 + (y-\xi)^2]^2} d\xi + \int_o^{\infty} \frac{\gamma \cdot H \cdot x^2}{[x^2 + (y-\xi)^2]^2} d\xi + \gamma \cdot g \cdot x \right) \quad (1)$$

$$\sigma_y = \frac{-2}{\pi} \left(\int_a^c \frac{\gamma \cdot H \cdot x \cdot (y-\xi)^2}{[x^2 + (y-\xi)^2]^2} d\xi + \int_c^e \frac{(\gamma \cdot H - K_1 \cdot \gamma \cdot H \cdot \xi - \frac{B \cdot \gamma \cdot H - K_1 \cdot h \cdot \gamma \cdot A}{A-B} \cdot x \cdot (y-\xi)^2)}{[x^2 + (y-\xi)^2]^2} d\xi + \int_e^g \frac{(\frac{K_1 \cdot \gamma \cdot H \cdot \xi - K_1 \cdot j \cdot \gamma \cdot C}{B-C} \cdot x \cdot (y-\xi)^2)}{[x^2 + (y-\xi)^2]^2} d\xi + \int_g^i \frac{(\frac{-K_2 \cdot \gamma \cdot H \cdot \xi + \frac{j \cdot \gamma \cdot C \cdot K_2}{C-D} \cdot x \cdot (y-\xi)^2)}{[x^2 + (y-\xi)^2]^2} d\xi + \int_i^o \frac{(\frac{K_2 \cdot \gamma \cdot H \cdot x \cdot (y-\xi)^2 - K_2 \cdot F \cdot \gamma \cdot H}{E-F} \cdot x \cdot (y-\xi)^2)}{[x^2 + (y-\xi)^2]^2} d\xi + \int_o^{\infty} \frac{(\frac{-K_1 \cdot \gamma \cdot H \cdot \xi + \frac{K_1 \cdot F \cdot \gamma \cdot H}{F-G} \cdot x \cdot (y-\xi)^2)}{[x^2 + (y-\xi)^2]^2} d\xi + \int_o^{\infty} \frac{(\frac{(\gamma \cdot H - K_1 \cdot \gamma \cdot H \cdot \xi + \frac{G \cdot \gamma \cdot H - K_1 \cdot l \cdot \gamma \cdot H}{G-I} \cdot x \cdot (y-\xi)^2)}{[x^2 + (y-\xi)^2]^2} d\xi + \int_o^{\infty} \frac{\gamma \cdot H \cdot x \cdot (y-\xi)^2}{[x^2 + (y-\xi)^2]^2} d\xi \right) \quad (2)$$

$$\tau_{xy} = \frac{-2}{\pi} \left(\int_a^c \frac{\gamma \cdot H \cdot x^2 \cdot (y-\xi)}{[x^2 + (y-\xi)^2]^2} d\xi + \int_c^e \frac{(\frac{\gamma \cdot H - K_1 \cdot \gamma \cdot H \cdot \xi - \frac{B \cdot \gamma \cdot H - K_1 \cdot h \cdot \gamma \cdot A}{A-B} \cdot x^2 \cdot (y-\xi)}{[x^2 + (y-\xi)^2]^2} d\xi + \int_e^g \frac{(\frac{K_1 \cdot \gamma \cdot H \cdot \xi - K_1 \cdot j \cdot \gamma \cdot C}{B-C} \cdot x^2 \cdot (y-\xi))}{[x^2 + (y-\xi)^2]^2} d\xi + \int_g^i \frac{(\frac{-K_2 \cdot \gamma \cdot H \cdot \xi + \frac{j \cdot \gamma \cdot C \cdot K_2}{C-D} \cdot x^2 \cdot (y-\xi)}{[x^2 + (y-\xi)^2]^2} d\xi + \int_i^o \frac{(\frac{K_2 \cdot \gamma \cdot H \cdot x^2 \cdot (y-\xi) - K_2 \cdot F \cdot \gamma \cdot H}{E-F} \cdot x^2 \cdot (y-\xi))}{[x^2 + (y-\xi)^2]^2} d\xi + \int_o^{\infty} \frac{(\frac{-K_1 \cdot \gamma \cdot H \cdot \xi + \frac{K_1 \cdot F \cdot \gamma \cdot H}{F-G} \cdot x^2 \cdot (y-\xi)}{[x^2 + (y-\xi)^2]^2} d\xi + \int_o^{\infty} \frac{(\frac{(\gamma \cdot H - K_1 \cdot \gamma \cdot H \cdot \xi + \frac{G \cdot \gamma \cdot H - K_1 \cdot l \cdot \gamma \cdot H}{G-I} \cdot x^2 \cdot (y-\xi))}{[x^2 + (y-\xi)^2]^2} d\xi + \int_o^{\infty} \frac{\gamma \cdot H \cdot x^2 \cdot (y-\xi)}{[x^2 + (y-\xi)^2]^2} d\xi \right) \quad (3)$$

where σ_x is the tension of the x-direction in the fault zone, MPa; σ_y is the stress of the y-direction in the fault zone; τ_{xy} is the shear stress of the fault zone, MPa; γ is the rock mass density, kg/m³; H is the buried depth of the working face roof, m; ξ is a variable; g is the gravity acceleration, N/kg; and K_1 and K_2 are the stress concentration and reduction coefficient, respectively. The specific meanings of the length units A, B, C, D, E, F, G, and I are shown in Fig. 1. The usual and shear stresses of the fault zone can be calculated as follows:

$$\sigma_N = \sigma_y \cdot \sin^2 \theta + \sigma_x \cdot \cos^2 \theta + 2 \sin \theta \cdot \cos \theta \cdot \tau_{xy} \quad (4)$$

$$\tau_N = \sin \theta \cdot \cos \theta \cdot (\sigma_x - \sigma_y) + (\sin^2 \theta - \cos^2 \theta) \cdot \tau_{xy} \quad (5)$$

where σ_N is the general stress of the fault zone; τ_N is the shear stress of the fault zone, MPa; and θ is the dip angle, °.

Because it is difficult to find an analytical solution with the above calculation equations, relevant parameters are assigned according to the actual coal mine site conditions, to analyze the stress distribution in the fault zone. The specific parameters selected are shown in Table 1.

Table 1. Parameter selection

Parameter	Value	Parameter	Value
Rock mass density γ	2.5Mg·m ⁻³	Buried depth of roof	600m
Distance between OA	120m	Distance between AB	30m
Distance between BC	10m	Distance between CD	10m
Distance between DE	50m	Distance between EF	10m
Distance between FG	10m	Distance between GI	30m
Fault dip angle	60°	Thickness of roof	190m
Stress concentration K_1	3.0	Reduction coefficient K_2	0.7

The parameters in Table 1 are substituted into equations (4) and (5) to obtain the stress distribution of the normal and shear stresses of the fault zone under spacing distances of 10, 30, 50, and 70m between the working surface and fault, as shown in Figure 2 and Figure 3.

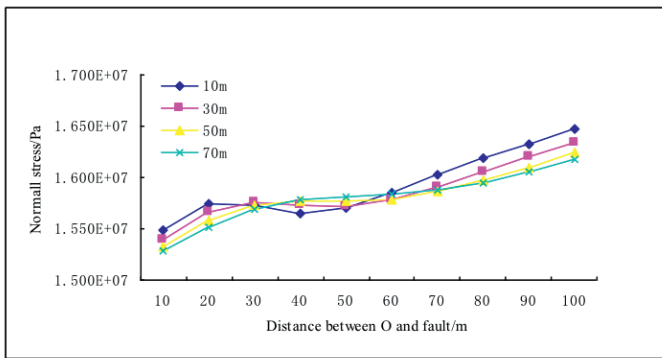


Figure 2. Normal stress distribution of the fault zone under different spacing distances

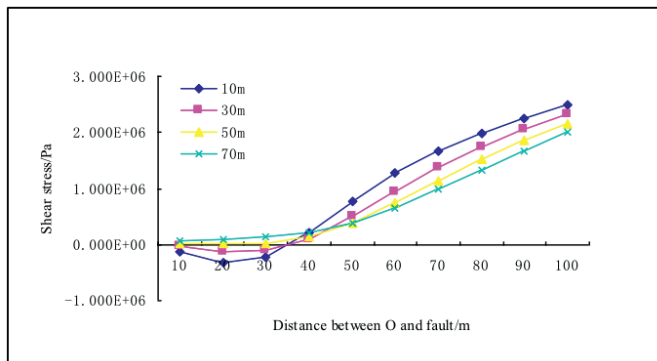


Figure 3. Shear stress distribution of the fault zone under different spacing distances

It can be observed from Figure 2 that the maximum normal stress value in the fault zone appears at a distance of 100m between the fault zone and origin O; that is, the closest position to the working face. Here, the normal stress of the fault zone is relatively large at most places under the condition that the working surface is 10m away from the fault; however, the stress is relatively small when the working surface is 70m away from the fault. At a distance of 30 to 40m, the normal stress is relatively large under the condition that the working surface is 70m away from the fault, while it is relatively small under the distance of 30m. It happens because the mining working surface is causing additional normal stress in the fault zone, and the closer the distance to the fault, the more significant the influence will be. It can be seen from Figure 3

that the maximum shear stress value in the fault zone is at 100m from the origin O under different distances between the working surface and fault; that is, the closest position to the working face. Here, the shear stress of the fault zone is relatively large at most places under the condition that the working surface is 10m away from the fault; however, the stress is relatively small where the working surface is 70m away from the fault. Likewise, the shear stress is relatively large under the condition that the working surface is 70m away from the fault, while it is relatively small at 30m, as a result of additional working surface shear stress. Combining Figure 2 with Figure 3, it can be seen that the working face mining stress has a significant effect on the fault zone, causing the changing trend of the normal and shear stresses of the fault zone first increasing and then decreasing, under the conditions that the working surface is 10 and 30m from the fault. The working face mining stress has a small effect on the fault zone, resulting in the changing trend of the normal and shear stresses of the fault zone increasing gradually, under distance conditions of 50 and 70m.

2.2. Numerical model analysis

A working face-mining-reverse-fault-simulation model was established by utilizing the numerical simulation software FLAC^{3D}, to better analyze the variation law of the fault zone under the influence of mining, as well as to verify the fault mechanics model analysis. The mining range of the model is 100m in length, 540m in trend length, and 100m in height, as illustrated in Figure 4.

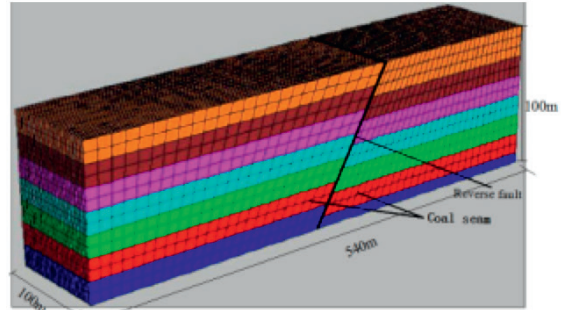


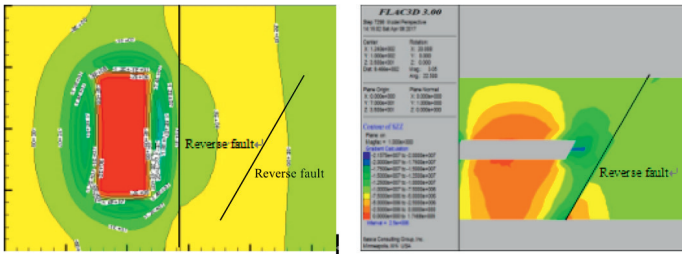
Figure 4. Numerical model

The working surface excavation process is simulated using dummy cells, using the Mohr-Coulomb model for simulating the mechanical changes in the coal and rock mass. Based on the geological survey and related rock mechanics test results, the rock mass size effect is taken into account. The parameters of each rock formation adopted in the simulating calculations are displayed in Table 2.

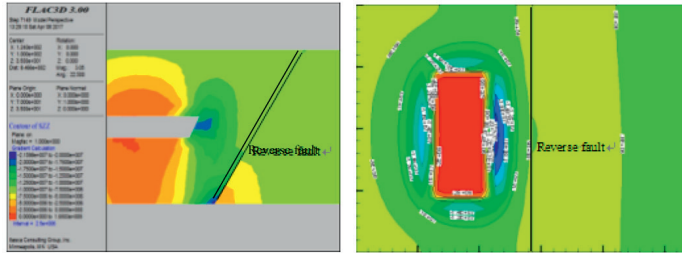
Table 2. Rock mechanical parameters

Lithology	Density /($\text{kg} \cdot \text{m}^{-3}$)	Bulk modulus /GPa	Shear modulus /GPa	Cohesion /MPa	Tensile strength /MPa	Internal friction angle (°)
Conglomerate	2530	13	8	1.5	2	37
Mudstone	2300	10	7	0.5	1.5	40
Coal	1500	10	6	1	1	20
Siltstone	2520	13	7	1.5	2	35
Magmatic	3000	70	50	2	25	45
Gristone	2550	15	8	8	12	25

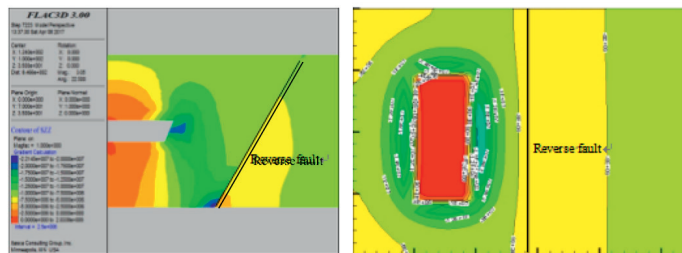
Based on the theoretical calculation scheme, a simulation scheme with distances of 10, 30, 50, and 70m between the working face and fault is established when the fault dip angle is 60°. The cross-section of the longitudinal section of the working face mining position and the roof plate horizontal position are intercepted to analyze the effects of the distance between the mining working surface and fault. The simulation results are displayed in Figure 5.



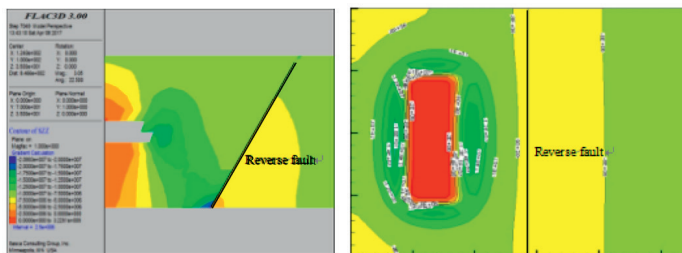
(a) Stress distribution with a distance of 10m between working face and fault



(b) Stress distribution with a distance of 30m between working face and fault



(c) Stress distribution with a distance of 50m between working face and fault



(d) Stress distribution with a distance of 70m between working face and fault

Figure 5. Stress distribution with different distances between working face and fault

It can be seen from the longitudinal section in Figure 5 that the stress concentration lies in the roof plate position on the front face of the working surface under four distance conditions between the working surface and fault. The stress in this position should be the maximum; the closer the distance to the fault, the larger the additional stress generated in the fault will be. This point is the same as the maximum position of the fault zone in the theoretical analysis. It can be seen from the horizontal cross-section in Figure 5 that when the working surface is 10 and 30m, respectively, from the fault, the roof plate stress range should cover the position of the fault zone, apparently affecting the fault zone stress. Under the distance conditions of 50 and 70m, the working surface stress range excludes the fault zone position.

According to the numerical simulation results, the influence of the mining stress on the fault zone stress is gradually reduced with an increase in the working distance between the working face and fault, which is also the case in the theoretical calculation. Therefore, when combining the elastic

mechanic's theory and numerical simulation results, it can be concluded that the working surface trending mechanics model of the working fault in the working face can be effectively reflected by the variation law of the fault zone stress.

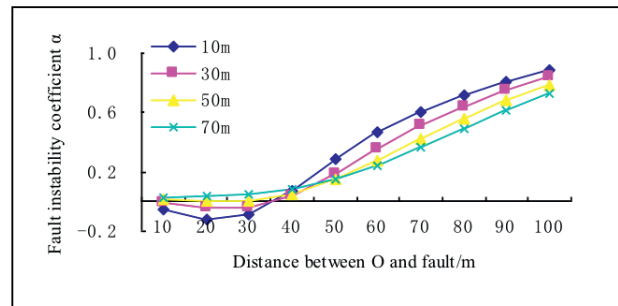
2.3 Stability analysis of reverse fault zone

Two methods for the Mohr-Coulomb strength criterion and fault activation determination were selected to analyze the fault stability. In determining the strength criterion, the fault friction angle is selected as 10° , and the cohesion is 0.1MPa. Since the friction angle and cohesive force of the fault are determined according to the empirical value, and the characteristics of each fault in the fault zone differ, the qualitative analysis could only be conducted on the possibility of fault instability, rather than determining whether the fault was stabilized. The fault instability coefficient is set as α , according to the Mohr-Coulomb theory strength criterion equation, to facilitate analysis, as is showed in Formula 6. The larger the value of α , the higher the probability of fault instability; the smaller the value of α , the more stable the fault will be. The fault activation determination method is conducted according to the ratio between the shear and normal stress of the fault zone; the more significant the ratio, the higher the possibility of instability.

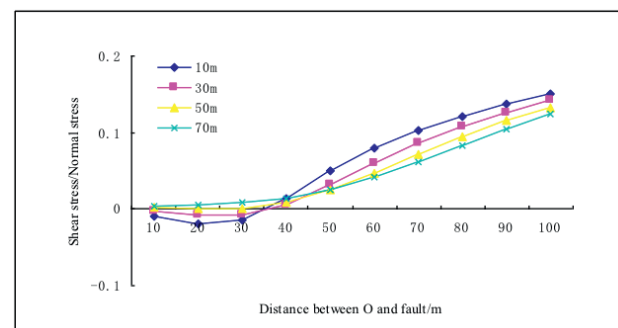
$$\alpha = \frac{\tau_N}{C_f + \sigma_N \cdot \tan \phi} \quad (6)$$

where C_f is the fault cohesion, MPa, and ϕ is the internal friction angle, $^\circ$.

Employing this calculation, when the distances between the working surface and fault are 10, 30, 50, and 70m, respectively, the ratio variation law among the instability coefficient of the reverse fault, the shear stress, and the normal stress can be obtained, as indicated in Fig. 6.



(a) Variation law of fault instability coefficient



(b) Variation law of shear stress with normal stress

Figure 6. Variation law of fault with different distances

It can be observed from Figure 6 that the fault stability results obtained by the two methods are almost the same. The position with poor stability in the fault zone is located at a distance of 100m between the fault zone and origin O; that is, the closest position to the working face. Here, the poorest fault stability is under the distance condition of 10m between the working surface and fault,

while the highest fault stability can be obtained at a distance of 70m. Under distance conditions of 50 and 70m between the working face and fault, the working face mining stress has no apparent effect on the fault zone; thus, the fault zone stability is gradually increased. Under distance conditions of 10 and 30m between the working face and fault, the working face mining stress results in apparent additional pressure on the fault zone, causing its overall stability to exhibit a trend of first increasing, then decreasing and growing again. Moreover, negative values exist in the calculation of the ratio of the instability coefficient, shear stress, and normal stress in the fault zone. The physical meaning of the fault zone is that the stress leading position of the fault is different from other areas. In this case, the possibility of fault fracture is also intensified, in opposition to fault stability. Therefore, such a stress state should be avoided in actual production work.

In summary, it is clear that the working face mining pressure significantly influences the fault stability. Moreover, the closer the fault, the higher this influence will be. Therefore, the minimum spacing between the working face and fault should firstly be determined in field work, to avoid the risk of fault instability caused by different stress directions in the fault zone. Then, comprehensive consideration should be given to actual situations, such as roof plate support on site and economic benefits, to reasonably determine the width of the coal pillar between the working face and reverse fault.

2.4 Analysis of actual situations on site

The 25110 working face of a particular mine consists of fully mechanized caving faces, located at the level of -445m of the mine 25 mining area. The 2-1 coal seam was evacuated on the working surface. The coal ranges from 7.4 to 13.8m in thickness, moving towards 112 to 27° with a tendency of 202 to 217° and a dip angle of 12°, and belongs to the slowly inclined thick coal seam. The lower lane of the working surface of 25011 is near the F16 reverse fault, as indicated in Figure 7.

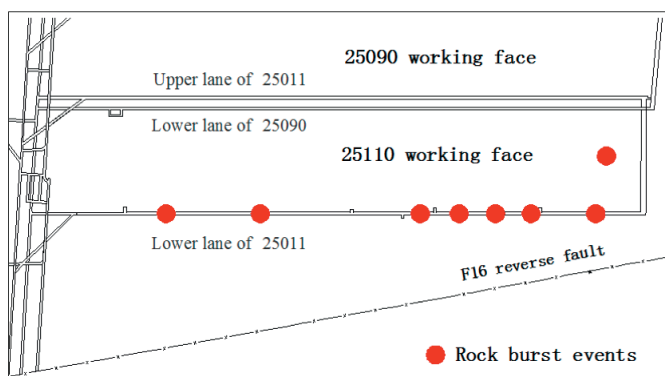


Figure 7. Layout of 25011 working face

According to the actual situation on site, a total of eight rock burst events occurred in the 25110 working face during the mining process, all within the lower lane of 25011. The first to seventh events occurred during the tunnelling process, while the eighth occurred during the mining process. Therefore, we can conclude that the 25011 lower lane approaching the reverse fault is a major area for rockburst occurrence. Furthermore, as the mining distance during the early stage approached the reverse fault, one rockburst event was also caused during the mining process; thereafter, no such event occurred. Thus, it can be determined that the closer the dip distance of the working face to the fault, the more easily the rock burst will occur, which is consistent with previous analysis results.

3 Conclusions

(1) Based on the law of the working face dip pressure distribution, a reverse fault mechanics analysis model was established to deduce the calculation equation of the normal and shear stresses of the fault zone under

the influence of the mining working face. It could be observed that the normal and shear stresses of the fault zone exhibited a changing trend of first increasing and then decreasing under the conditions in which the working surface was 10 and 30m from the fault. The normal and shear stresses of the fault zone were exhibited a changing trend of increasing gradually under distance conditions of 50 and 70m between the working surface and fault. The stress distribution of the longitudinal and transverse horizontal sections under spacing conditions of 10, 30, 50, and 70m between the working and fault distance were obtained by means of the FLAC^{3D} numerical simulation method. The results indicate that the influence range of the mining stress on the working face at spacing distances of 10 and 30m included the fault zone, while at spacing distances of 50 and 70m, the fault zone was excluded. Consequently, it can be concluded that the mining stress not only affects the fault zone, but also changes the variation trend of its normal and shear stresses under spacing conditions of 10 and 30m; however, there was less influence under spacing conditions of 50 and 70m.

(2) Two Mohr-Coulomb theory rule methods and fault activation determination were applied to analyse the fault zone stability. When the working surface was 10 and 30m away from the fault, negative values existed in the calculation of the instability coefficient, shear stress, and normal stress ratio in the fault zone. The physical meaning of the fault zone is that the stress leading position of the fault is different from other positions. In such a case, the possibility of fault fracture is also intensified, resulting in a possibility of rock burst. When the spacing was 50 and 70m, the fault zone stability exhibited an overall changing trend of gradually increasing. Moreover, the most dangerous fault zone positions under four spacing conditions were located at the closest position to the fault.

(3) Based on actual site conditions, rock burst was more likely to occur in the lanes approaching the fault zone, indicating that the spacing between the working surface and fault zone was an important factor affecting the occurrence of rock burst. Therefore, determining a reasonable distance between the mining working face and inverse fault zone was a foundation for preventing rock burst.

Acknowledgments

This research was financially supported by the Yong Foundation of China Coal Technology Engineering Group (No. 2014QN003); the State Key Research Development Program of China (No. 2016YFC0801605); the National Natural Science Foundation of China (No. 51674061); and the State Key Research Development Program of China (No. 2016YFC0600706).

References

- Asghar, Z., Ali, W., Nasir, A., & Arshad, A. (2018). Atmospheric Monitoring for Ambient Air Quality Parameters and Source Apportionment of City Faisalabad, Pakistan. *Earth Sciences Pakistan*, 2(1), 01-04.
- Diaz-Aguado, M. B., & González-Nicieza, C. (2007). Control and prevention of gas outbursts in coal mines, Riosa-Olloniego coalfield, Spain. *International Journal of Coal Geology*, 69, 253-266.
- Gibowicz, S. J. (1984). The mechanism of large mining tremors in Poland(1984). *Rockbursts and seismicity in mines*, 22, :17-28.
- Guan Leong, T., Tahir, S.H. & Asis, J. (2018). Stratigraphy of Paleogene Sequences in Weston – Sipitang, Sabah. *Geological Behavior*, 2(1), 01-04.
- Jiang, F. X., & Liu, W. J. (2010). Coupling study of microseismic monitoring and numerical simulation for tectonic activation. *Journal of China Coal Society*, 35, 900-904.
- Jiang, Y. D., Pan, Y. S., Jiang, F. X., Dou, L. M., & Ju, Y. (2014). State of the art review on mechanism and prevention of coal bumps in China. *Journal of China Coal Society*, 39, 205-213.
- Jiang Fuxing, LIU Weijian. Coupling study of microseismic monitoring and numerical simulation for tectonic activation.(2010). *Journal of China Coal Society*, 35: 900-904.
- Jiang Yaodong, Pan Yishan, Jiang Fuxing, et al. (2014) State of the art review on mechanism and prevention of coal bumps in China. *Journal of China Coal Society*, 39: 205—213.
- Joughin, N. C., & Jager, A. J. (1984). Fracture of rock at stope faces in South African gold mines. *Proceedings of Symposium of Rockbursts*:

- prediction and Control, 27, 53 -66.
- Khanchoul, K., Saaidia, B., & Altschul, R. (2018). Variation in Sediment Concentration and Water Discharge During Storm Events in Two Catchments, Northeast of Algeria. *Earth Sciences Malaysia*, 2(2), 01-09.
- James W, LaMoreaux, J. W., Wu, Q., & Zhou, W. (2014) New development in theory and practice in mine water control in China. *Carbonates and Evaporites* 29, :141–145.
- Li, Z. L., Dou, L. M., Cai, W., Wang, G. F., He, J., Gong, S. Y., and & Ding, Y. L., (2014)., Investigation and analysis of the rock burst mechanism induced within fault-pillars. *International Journal of Rock Mechanics and Mining Sciences*, 70, 192–200.
- Mahmood, S., Kazmi, S.T., & Ali, S.S. (2018). Comparison of Drinking Water Bottles of Different Countries Along with Zamzam Water, Pakistan. *Earth Sciences Pakistan*, 2(1), 05-14.
- María B, Díaz A, González NC (2007) Control and prevention of gas outbursts in coal mines, Riosa–Olloniego coalfield, Spain. *Int J Coal Geol* 69:253–266.
- McGarr, A. (1984). Some applications of seismic source mechanism studies to assessing underground hazard(1984). *Rockbursts and seismicity in mines*, 31, : 199-208.
- Nwankwoala, H.O., & Ememu, A.J. (2018). Hydrogeochemical Signatures and Quality Assessment of Groundwater in Okpoko And Environs, Southeastern Nigeria. *Pakistan Journal of Geology*, 2(1), 06-11.
- Potgieter, G. J., & Roering, C. (1984). The influence of geology on the mechanisms of mining-associated seismicity in the Klerksdrop gold-field.(1984) *Rockbursts and seismicity in mines*, 11, 1984 : 45 -50.
- Qian, M. G. (2003). *Minggao, Shi Pingwu, Ground Pressure and Strata Control*. (Xuzhou: China University of Mining and Technology press.,2003)
- Rahim, I.A., Asis, J., & Mohd Husin, M.A.Y. (2018). Comparison of Different Type of Friction Angle in Kinematic Analysis. *Malaysian Journal of Geosciences*, 2(1), 35-38.
- Sudhakaran, M., Ramamoorthy, D., Savitha, V., & Balamurugan, S. (2018). Assessment of trace elements and its influence on physio-chemical and biological properties in coastal agroecosystem soil, Puducherry region. *Geology, Ecology, and Landscapes*, 2(3), 169-176.
- Sufiyan, I., Zakariya, R., Yacoob, R., Idris, M.S., & Idris, N.M. (2018). SWAT Subbasins Parameters and Flood Risk Simulations Using 3d In Terengganu Watershed. *Earth Sciences Malaysia*, 2(2), 10-15.
- Tair, R. & Dell, L. (2018). Spring-Water as An Alternative Resource After Earthquake for Villagers, Kota Belud Sabah. *Geological Behavior*, 2(1), 05-11.
- Tan, Y. L., Ning, J. G., & Zhao, T. B., (2011). *Deformation and control of deep roadways*. (Beijing: Coal Industry Press., 2011),
- Thiruchelvam, S., Ismail, M.F., Ghazali, A., Mustapha, K.N., Norkhairi, F.F., Yahya, N., Isa, A.M.M., & Muda, Z.C. (2018). Development of Humanitraian Supply Chain Performance Conceptual Framework in Creating Resilient Logistics Network. *Malaysian Journal of Geosciences*, 2(1), 27-30.
- Veeraragavan, S., Duraisamy, R., & Mani, S. (2018). Seasonal variation of soil enzyme activities in relation to nutrient and carbon cycling in Senna alata (L.) Roxb invaded sites of Puducherry region, India. *Geology, Ecology, and Landscapes*, 2(3), 155-168.
- Wali, E., Phil-Eze, P.O., & Nwankwoala, H.O. (2018). Forecasting the Future Pattern of Land Use and Land Cover Change in The Wetland Ecosystem of The Port Harcourt Metropolis. *Pakistan Journal of Geology*, 2(1), 01-05.
- Xiao, Y. X., Feng, X. T., Li, S. J., Feng, G. L., & Yu, Y. (2016). Rock mass failure mechanisms during the evolution process of rockbursts in tunnels. *International Journal of Rock Mechanics and Mining Sciences*, 83,174-181.